Application of a Composite Material Shell-Element Model in Ballistic Impact and Crush Simulations

Tobias Achstetter, Kelly Carney, Paul Du Bois, Cing-Dao Kan
George Mason University
Sheng Dong
The Ohio State University
Allen Sheldon
Honda R&D Americas

Abstract

A new orthotropic material model with tabulated hardening curves for different loading directions, strain-rate and temperature dependency, damage, and a new strain-based generalized tabulated failure criterion was utilized to simulate ballistic impacts and a C-channel under crush loading. These validation simulations of the material model were performed to test the physical usefulness and robustness of the developed material model.
Ballistic impact tests were chosen to highlight the capabilities of the material model in high speed impact applications. For the tested unidirectional composite material in the ballistic impact, extensive material data was available.
In a recent study, Dong et al. calibrated an existing material model in crush simulations to match force-displacement characteristics of several crush experiments and a match between tests and simulations was achieved after several rounds of optimization. To highlight the capabilities of the new material model in crush load cases, its results were compared to the force-time history obtained in tests and simulations using MAT58.
For both the ballistic impact and crush simulations, the same modeling approach was used.

Ballistic Impact Loadcase

Several high velocity ballistic impact tests were conducted at NASA Glenn Research Center (NASA-GRC) to validate the developed material model [1]. Square 16 ply unidirectional T800/F3900 composite panels with the dimensions of 12" x 12" x 0.122" were impacted by projectiles with the weight of approximately 50 grams. The composite panels were manufactured with a layup of $[0, 90, +45, -45]_{2S}$. The cylindrical clamping of the panel had an inner radius of 5" and an outer radius of 6".

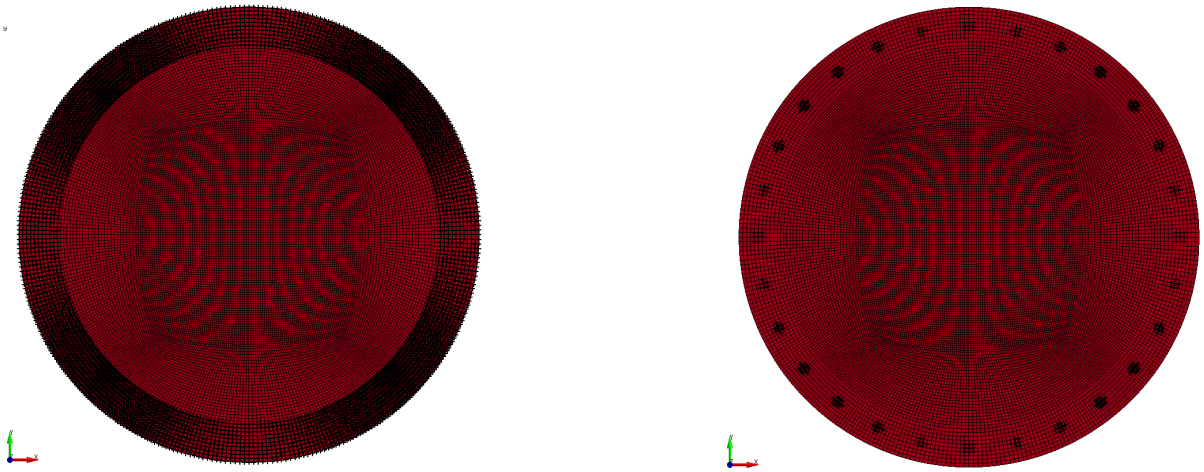

a) Clamping region, constrained in Z *b) Bolt holes, constrained in XY*

Figure 1: Boundary conditions of the plate in the ballistic impact simulation

In the simulation model, the square plate was modeled as a round plate that covered the region of the clamping. The overhanging parts of the plate were not modeled, as they were not considered to be important to the overall behavior of the plate. The panel was meshed relatively coarsely in the clamping region while using a finer mesh in the impact region. Based on the physical tests, the simulations were set up with single point constraints in the region of the clamping. Figure 1 shows the simulation setup to replicate the real-life boundary conditions without having to rely on modeling of the clamping plates to reduce the CPU time of the simulations. The bolts in the test were simulated by constraining the nodes in the bolt holes in-plane (Figure 1b), while the nodes on top and on the bottom of the plate in the clamping region were constrained out-of-plane (in impact direction, see Figure 1a).

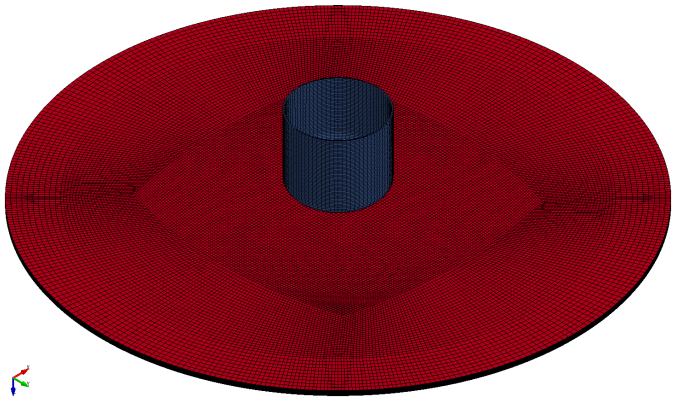

Figure 2: Isometric view of the ballistic impact simulation setup

The projectile then impacts the plate in the center of the panel, as shown in an isometric view of the simulation setup in Figure 2. Every ply of the composite layup was modeled with an individual shell element while also accounting for delamination by modeling the interface between the plies using cohesive elements. Figure 3 on the left shows the layup of the shell elements with their thickness shown and on the right with only the mid-plane of the shell elements.

Table 1: Cohesive material properties

LS-DYNA® variable	Description	Value
EN	Normal stiffness	6.16e 8 [psi / in]
ET	In-plane stiffness	6.16e 8 [psi / in]
GIC	Energy release rate for mode I	4.28 [psi · in]
GIIC	Energy release rate for mode II	14.5 [psi · in]
XMU	Exponent of the mixed mode criteria	1.0 [−]
T	Peak traction in normal direction	4000 [psi]
S	Peak traction in tangential direction	8000 [psi]

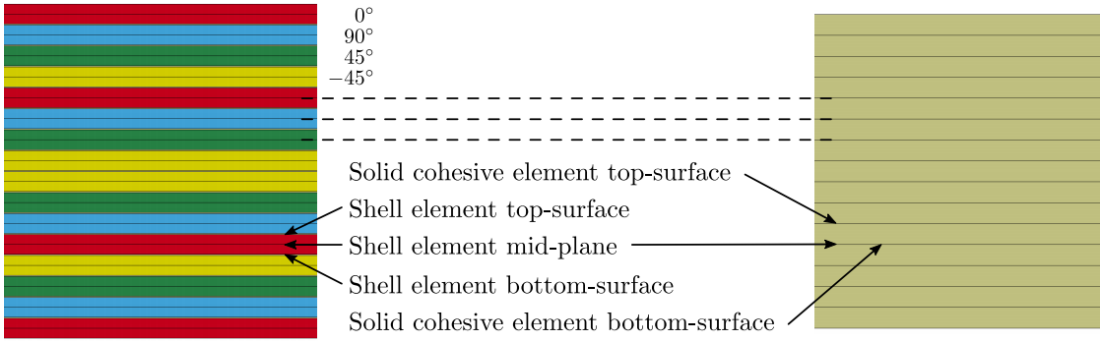

Figure 3: Composite plate layup and modeling technique with cohesive elements

The solid cohesive elements share the nodes with the shell elements and the cohesive material model chosen was *MAT_COHESIVE_MIXED_MODE (MAT138). Table 1 lists the material property values after they were adjusted to match DCB and ENF tests.

Table 2: LVG ballistic impact tests, impact and rebound/exit velocities (rounded)

Test ID	Impact Velocity [ft/s]	Rebound velocity [ft/s]	Exit velocity [ft/s]
LVG1065	116	69	-
LVG1067	155	84	-
LVG1073	172	89	-
LVG1069	178	79	-
LVG1070	181	94	-
LVG1068	182	97	-
LVG1066	185	104	-
LVG1064	237	116	-
LVG1075	**385**	**46**	**-**
LVG1074	**417**	**-**	**25**
LVG1076	**453**	**-**	**114**
LVG1063	535	-	263

In Table 2 all ballistic impact tests conducted by NASA-GRC are listed, sorted by impact velocities. For the lower velocities of 116 ft/s up to 384 ft/s, the projectile rebounded off the plate with the velocity shown in the “Rebound Velocity” column. The higher velocities from 417 ft/s to 535 ft/s penetrated the plate and exited with a velocity as shown in the column “Exit velocity”. The impact velocities of the tests LVG1075, LVG1074 and LVG1076 (highlighted in bolt font) were chosen to be simulated as they were in the region of the ballistic limit velocity, the highest impact velocity at which the plate is able to contain the projectile. Additionally, an impact velocity between LVG1075 and LVG1075, 406 ft/s, was simulated to verify that consistent results in the region of the ballistic limit velocity are obtained.

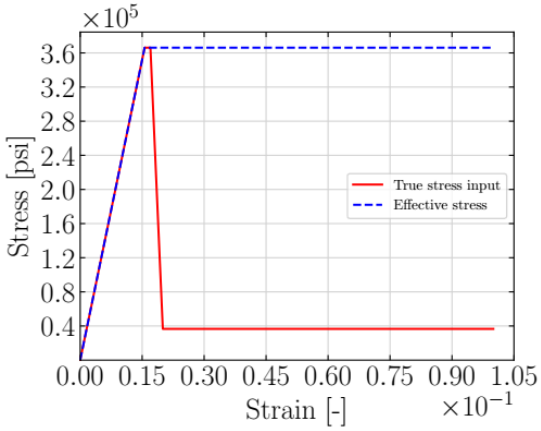

a) Tension 1-direction stress vs. strain input

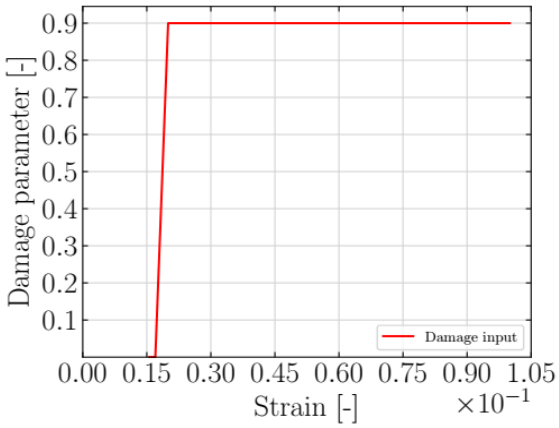

b) Tension 1-direction damage vs. strain input

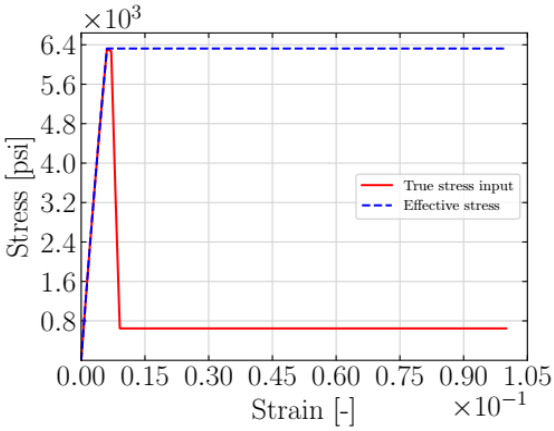

c) Tension 2-direction stress vs. strain input

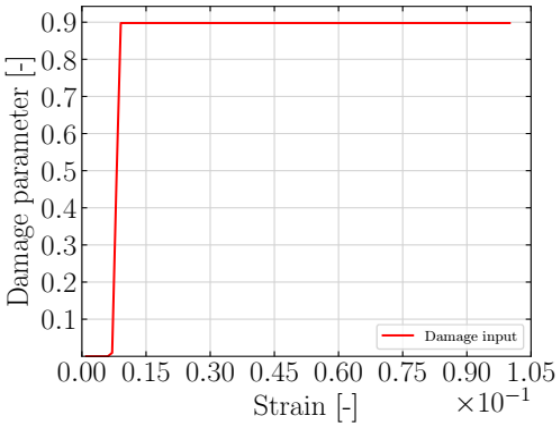

d) Tension 2-direction damage vs. strain input

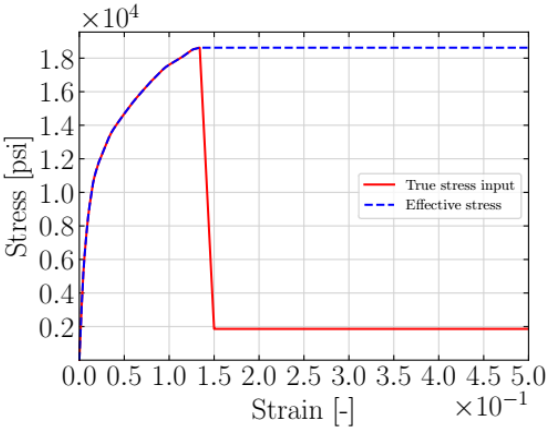

e) Shear 12-direction stress vs. strain input

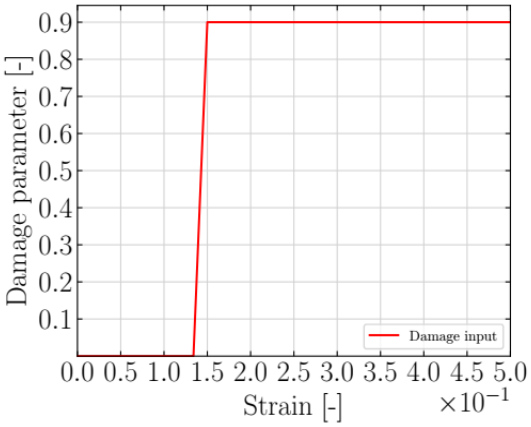

f) Shear 12-direction damage vs. strain input

Figure 4: Ballistic impact simulation material model input

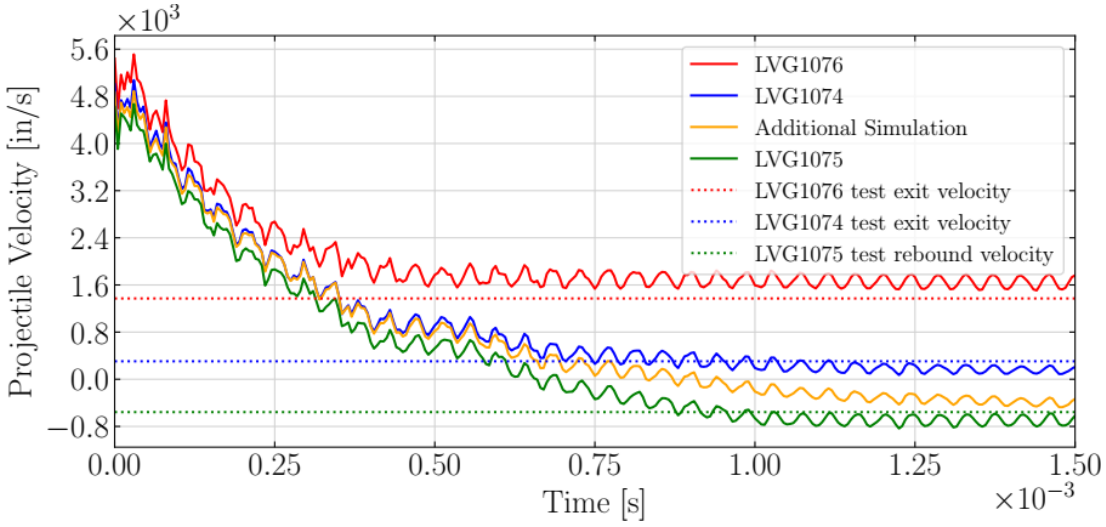

Figure 5: Projectile velocities in the LVG impact tests and simulations

In finite element simulations, failure of materials is generally modeled by eroding elements when stresses or strains reach a critical level. In engineering materials, when physical material tests are conducted, the test is usually stopped once the force drops, which is considered as "failure'" for the material. Composite materials, however, might still be able to take load in the other material directions. Consider, for example, a tensile load transverse to the fibers that leads to damage by debonding between fibers and the matrix material. The material is now considered to have "failed'", however, most fibers will still be intact, and the material could very well still take tensile loads in the fiber direction. If in a finite element simulation the element that reached that critical stress or strain in tension 2-direction is now eroded, the load bearing capabilities in other directions would be lost as well. The finite element should therefore not be eroded once the "failure" strain measured in uniaxial tension and compression tests is reached. Instead, in this validation study, the implemented damage model was used to degrade the stress in the direction where the "failure" strain from the uniaxial test occurred.

The stiffness and stress were degraded to a level of 10% of the maximum stress and stiffness and the element therefore lost most of its load bearing capabilities in this direction while maintaining it in others. Figure 4 shows the stress versus strain and damage input to the material model that achieved this behavior. A true stress versus strain (red) and an effective stress versus strain curve (dashed blue) were defined as shown in Figure 4a. From these curves, the damage versus strain curve was computed (Figure 4b), which converted the true stress curve into the monotonically increasing effective stress curve.

Input to the material model were then the true stress versus strain curve and the damage curve for the uncoupled damage term. Similarly, the input for tension 2-direction and 12-shear is prepared as shown in Figure Figure 4c through Figure 4f. The stress versus strain input for compression in 1 and 2-direction was left unchanged from the material test data [2].

As previously described, elements should not be eroded once the critical stress or strain is reached in a single loading direction. However, as in ballistic impacts where the projectile might fully penetrate the plate, some erosion of elements inevitably needs to take place to create the opening for the projectile. The newly developed Generalized Tabulated Failure Criterion was used to define a high equivalent erosion strain of 80% in all loading conditions by defining two curves with two angles each (-180° and 180°) with a corresponding equivalent erosion strain of 0.8 for both angles.

Only when the element deforms very drastically will it erode to avoid numerical instabilities and to allow for the projectile to penetrate the plate. The material input was the same in the three ballistic impact simulations.

Figure 5 shows the projectile velocities over time for the simulations. A positive velocity indicates the projectile was traveling forward, while a negative velocity can be observed for a rebounding projectile. The solid red line represents the velocity in the LVG1076 simulation over time, while the horizontal dashed red line marks the exit velocity of 114 ft/s (1368 in/s) that was measured in the physical impact test. The projectile initially had the impact velocity of 453 ft/s (5436 in/s) and was then slowed down while penetrating the composite plate. It exited the plate with a velocity 6.2% of the delta v higher than the measured velocity. However, if the physical test was repeated several times at the exact same velocity, the variation in the results would likely be higher than the difference between the test and simulation. In both the LVG1074 and LVG1075 simulations, the projectile velocity at the end of the simulation was 3.1% of the delta v below the measured exit velocity (LVG1074) and rebound velocity (LVG1075).

The difference between test and simulation was again relatively small, and the measured variations in tests would likely be higher. The additional simulated impact velocity between LVG1075 and LVG1074 of 406 ft/s (4872 in/s) shows a resultant rebound velocity that falls between the rebound and exit velocities of LVG1075 and LVG1074 (orange curve in Figure 5).

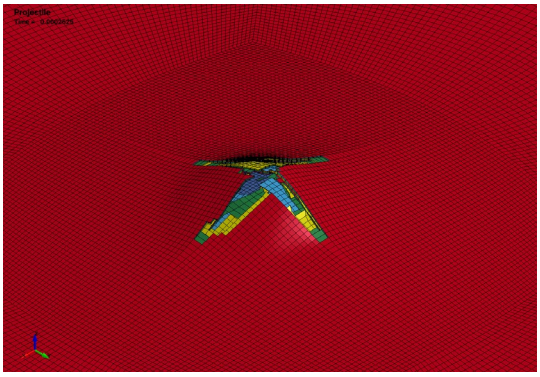

a) t = 0.00025s

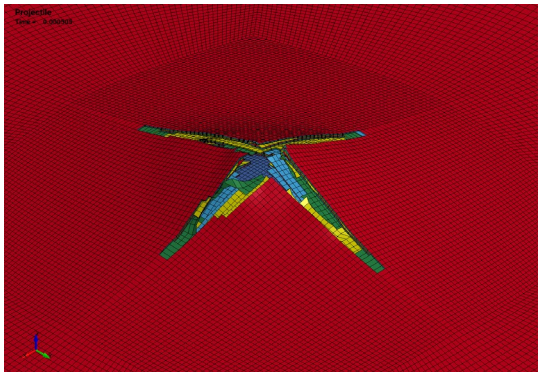

b) t = 0.00050s

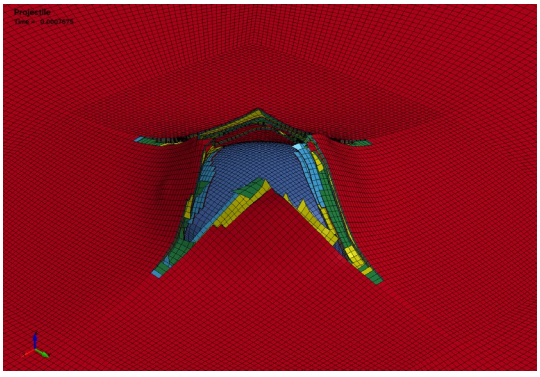

c) t = 0.00075s

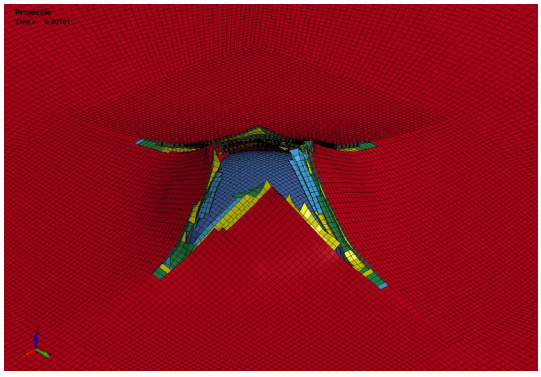

d) t = 0.00100s

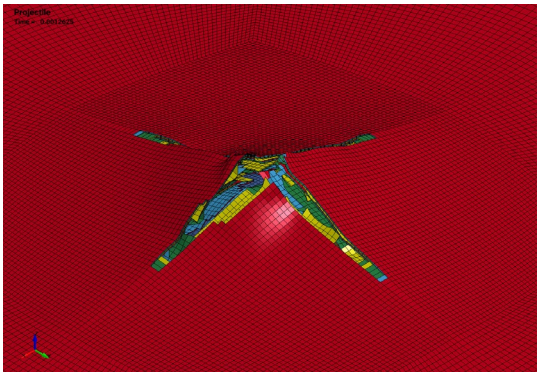

e) t = 0.00125s

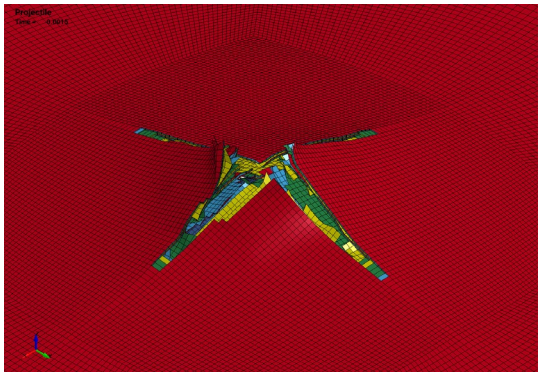

f) t=0.00150s

Figure 6: LVG1075 ballistic impact simulation

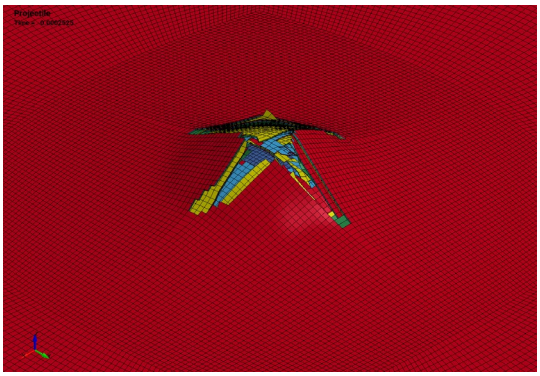

a) t = 0.00025s

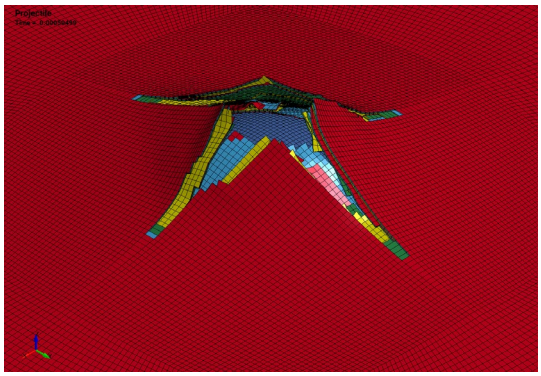

b) t = 0.00050s

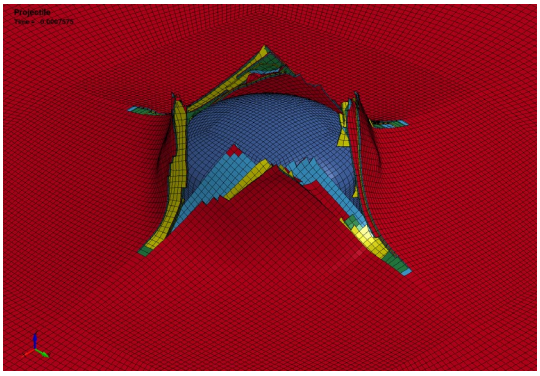

c) t = 0.00075s

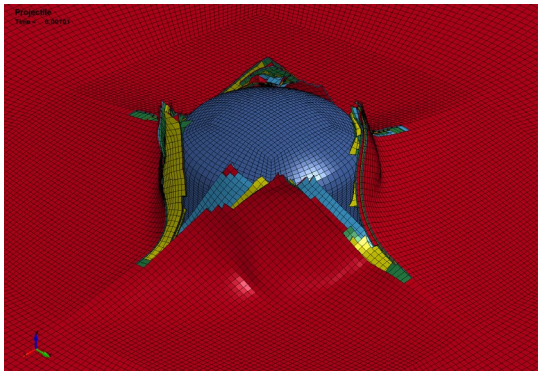

d) t = 0.00100s

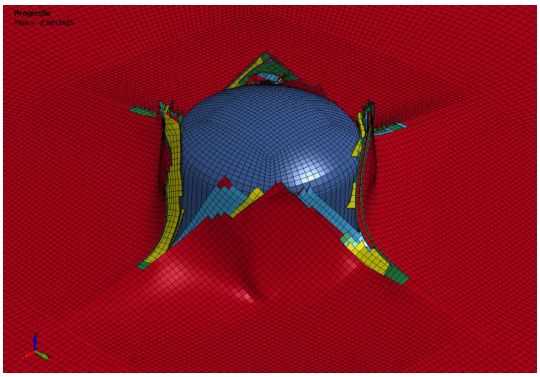

e) t = 0.00125s

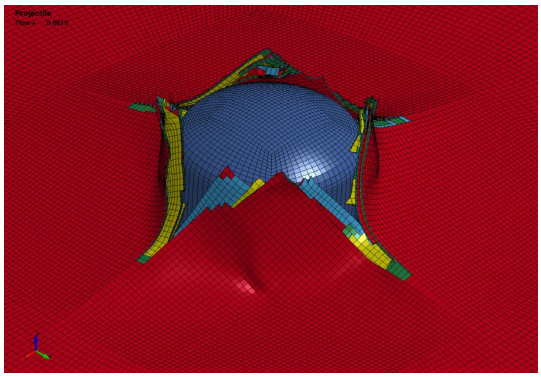

f) t=0.00150s

Figure 7: LVG1074 ballistic impact simulation

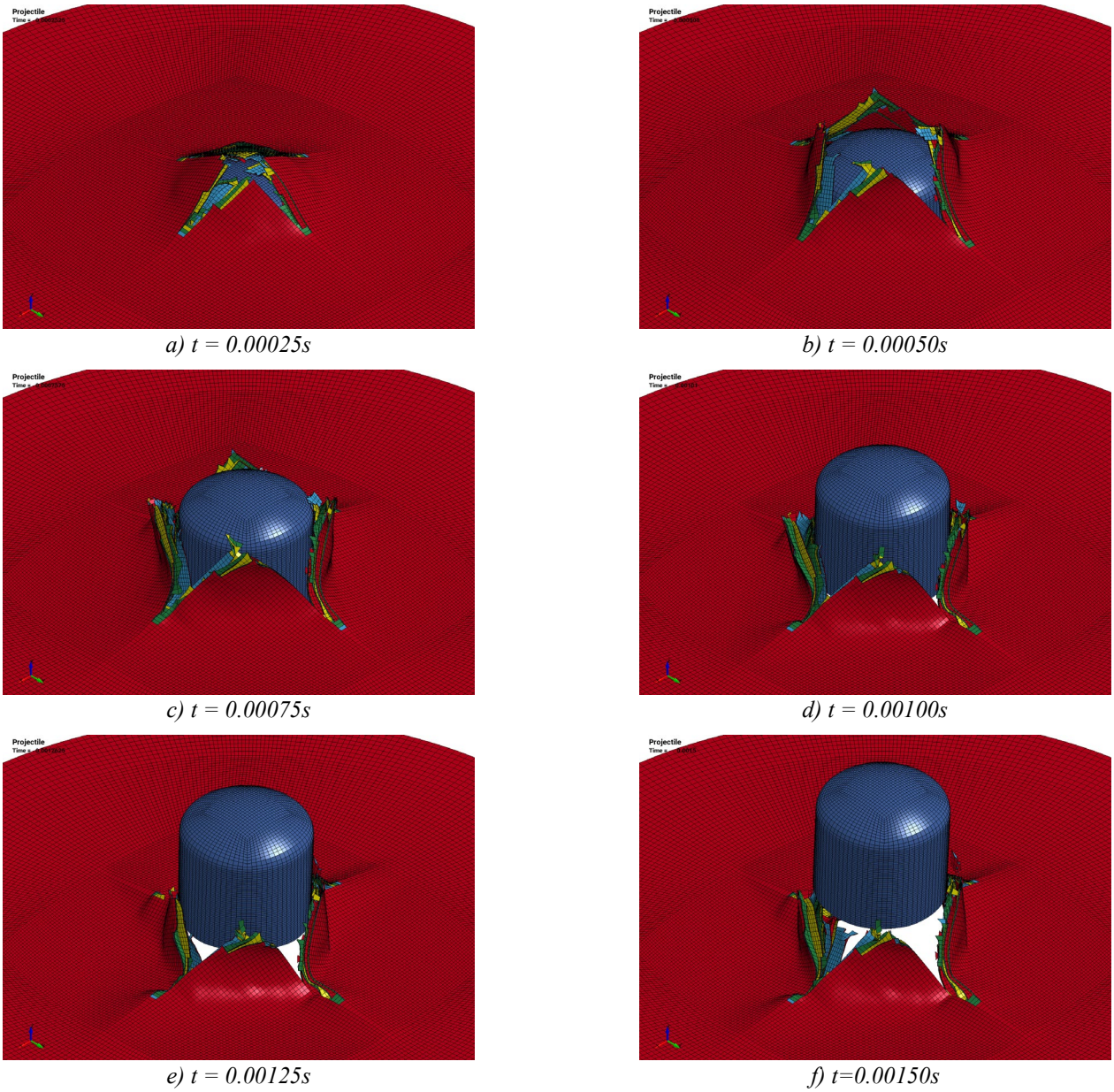

a) t = 0.00025s *b) t = 0.00050s*

c) t = 0.00075s *d) t = 0.00100s*

e) t = 0.00125s *f) t=0.00150s*

Figure 8: LVG1076 ballistic impact simulation

Figure 6 shows isometric views of the impacted region on the back side of the plate in the LVG1075 simulation, where, in the physical test, the projectile rebounded the plate with a relatively low velocity of 46 ft/s.

In the simulation, the projectile caused significant damage to the plate leading to rupture in a “cross-like” pattern. However, the projectile did rebound the plate in the simulation, similarly to the test.

Figure 7 shows isometric views of the impacted region on the back side of the plate in the LVG1074 simulation, where, in the physical test, the projectile penetrated the plate and exited with a relatively low velocity of 25 ft/s.

In the simulation, similar to the lower velocity (LVG1075) analysis, the plate again ruptured in a similar pattern. However, as the velocity plot in Figure 5 showed, the projectile then continued to travel forward with a positive velocity, similar to that of the test.

Figure 8 shows isometric views of the impacted region on the back side of the plate in the LVG1076 simulation, where, in the physical test, the projectile penetrated the plate and exited with a velocity of 114 ft/s. As in the test, the projectile ruptured the plate and exited through the back side. The initial velocity was significantly reduced, and the exit velocity matched the measured test velocity fairly well.

The failure patterns in the three different tests were relatively similar, as such, only one exemplary test result is compared to the patterns obtained in the corresponding simulation. Figure 9a shows the impacted side of the composite plate post-test at the LVG1076 impact velocity with a vertical fiber direction in the top ply.

Figure 9b shows the corresponding view at the last simulation time state. Visualization of deformation is turned off in the simulation image to show the exact failure pattern. While the test images represent the state of the plate after the projectile has long passed through the plate, simulating the rebound of the opening in the plate in the simulation would require very long time scales that cannot be simulated efficiently. The elements highlighted in turquoise are the eroded elements, while the elements highlighted in red show the maximum damage value (0.9) that the element reached. Apart from the "cross-like" failure pattern in both test and simulation, elements that were highly damaged along the fiber direction of the top ply can be seen extending up and down vertically from the horizontal crack.

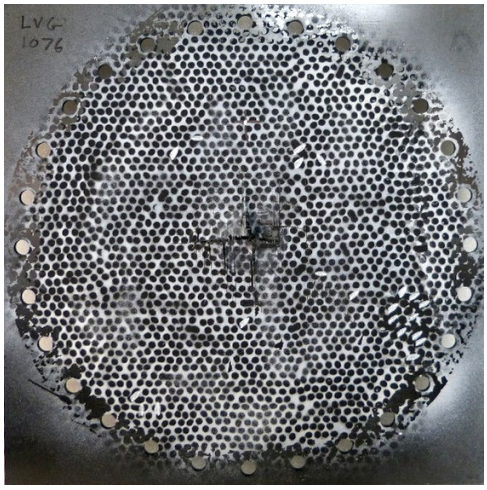

a) Test impacted side

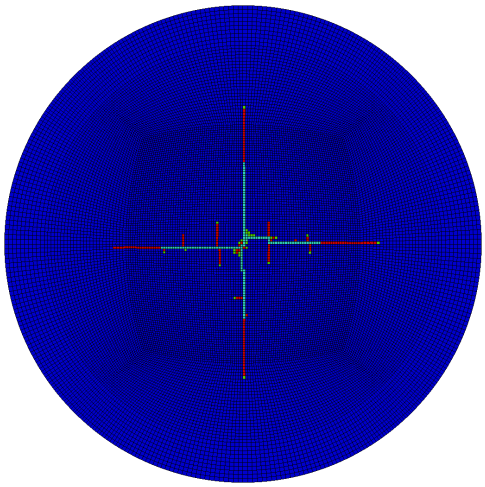

b) Simulation impacted side

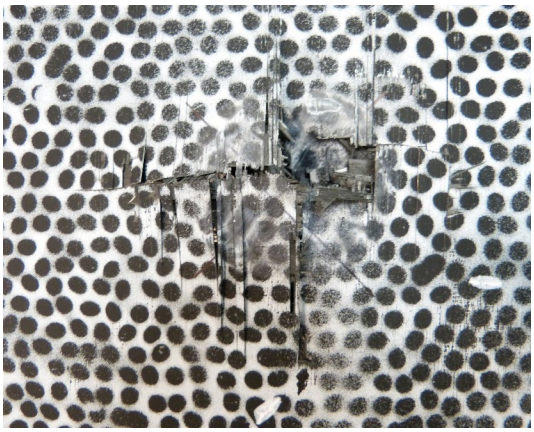

c) Test impacted side (zoom)

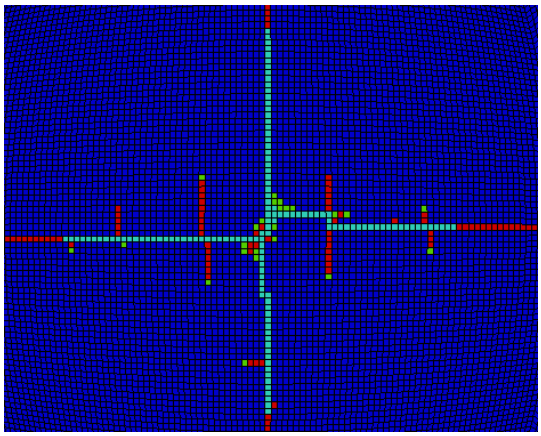

d) Simulation impacted side (zoom)

Figure 9: LVG1076 ballistic impact, failure patterns on impact side, test versus simulation

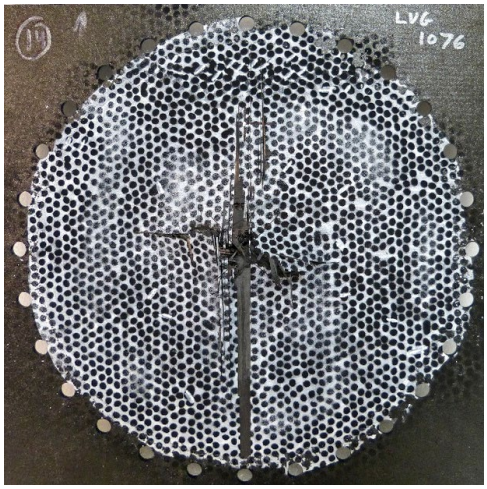

a) Test back side

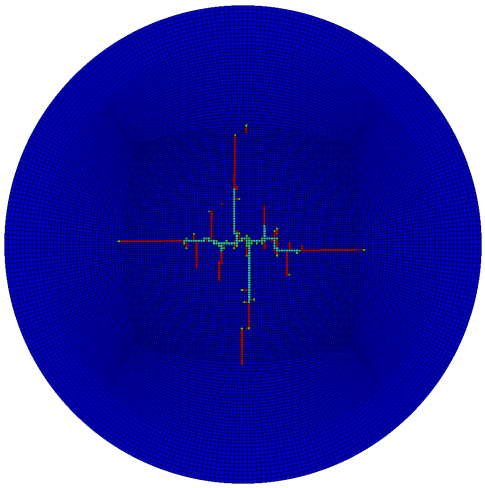

b) Simulation back side

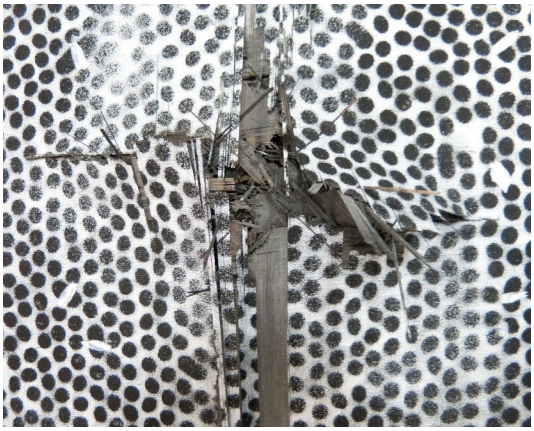

c) Test back side (zoom)

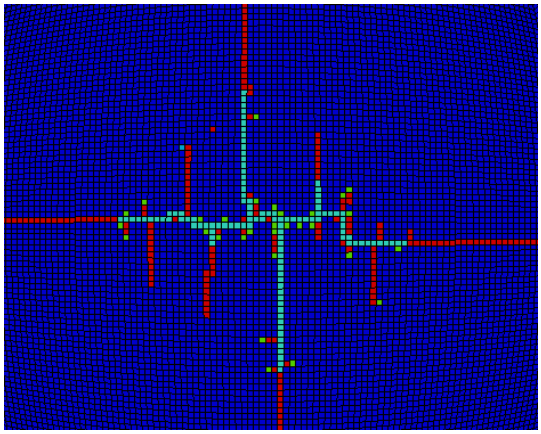

d) Simulation back side (zoom)

Figure 10: LVG1076 ballistic impact, failure patterns on back side, test versus simulation

In the simulation these damaged elements correspond to similar vertical cracks best seen in Figure 9c, which shows a zoomed in view of Figure 9a. As a comparison to this zoomed view of the test specimen, Figure 9d depicts a close-up view of the same area in the simulation. Similar images of the back side of the composite plate are shown in Figure 10. The fiber direction of the ply facing the camera is again aligned vertically. A “cross-like” fracture pattern can be seen in both the test and the simulation. In the test, damage in the top ply extended close to the clamping region of the plate with parts of this ply being completely separated from the plate. In the simulation, the damaged region also extended further outward in the fiber direction, and transverse to the fibers, showed a similar pattern as in the test. The small vertical fractures parallel to the fibers, similar to the ply facing the impact side, are again visible in both the test and the simulation.

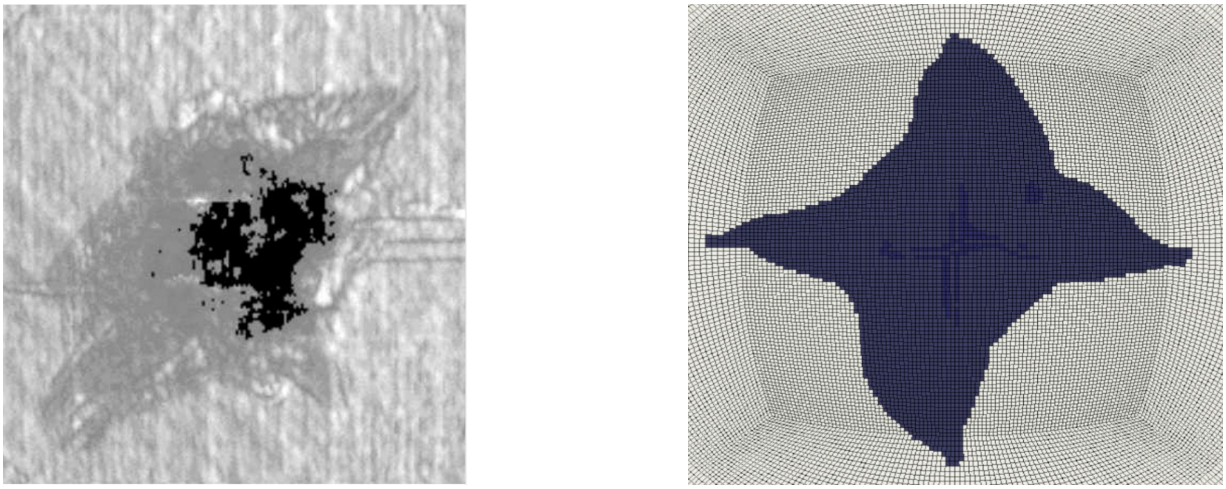

a) Test CT scan *b) Simulation, cohesive elements at 90% transparency*

Figure 11: LVG1074 ballistic impact, delamination, test versus simulation

Figure 11 shows a CT scan of the delaminated area in the LVG1074 impact test. To compare the delaminated area in the simulation, the eroded cohesive elements are highlighted in blue while making the cohesive part 90% transparent. This makes delaminated areas in all plies visible, similar to the CT scan. In the test and simulation delamination covered a similar area, while the shape seemed to be rotated about 45°. This might be an attribute of mesh dependency and alignment; further research to identify the causes would have to be conducted.

For all three impact velocities, a good agreement between the projectile velocity and failure patterns in test and simulation was achieved. The only parameter that had to be adjusted to match test and simulations was the equivalent erosion strain due to lack of experimental data. With more available data on uncoupled and coupled damage terms, the sensitivity of the erosion strain might diminish and make the material model more predictive.

Overall, the capabilities to accurately and robustly model ballistic impacts with the shell element material model were shown.

Crush Loadcase

To reduce weight and increase specific energy absorption of components subjected to crush loading, composite materials have properties that make them valuable in such scenarios. In the best case, a composite component that crushes due to progressive splaying, fragmentation, and localized delamination, can absorb large amounts of energy. If, however, the crushing is not ideally initialized, buckling and global breakage of the part can occur, which reduces the energy absorbing capabilities of the component [3].

In a recent study, Dong et al. calibrated a material model in crush simulations using an adaptive meta-model based on a global optimization strategy to match force-displacement characteristics of several crush experiments [3]. The samples in the study were manufactured using Vacuum assisted Resin Transfer molding (VaRTM) to infuse dry carbon fibers with a low viscosity epoxy resin [3].

The LS-DYNA material model that was calibrated in the study was the continuum damage mechanics model MAT58 and a match between tests and simulations was achieved after several rounds of optimization.

To highlight the capabilities of the new material model, its results were compared to the force-time history obtained by Dong et al. in simulations using MAT58. The material test data that was available at the time of this study did not provide all required information to fully define all necessary inputs for the new material model. For example, test data for compression in fiber and transverse direction was not available. Some of the inputs were therefore defined based on experience from other material combinations of fiber matrix pairings or directly derived from the validated material input used by Dong et al. [3].

Tension in fiber and transverse direction was modeled with the stress and stiffness being degraded to 10% once the maximum stress was reached. Test data was available for the in-plane shear direction and, therefore, the actual test data was used with the stress and stiffness being degraded to 10% after reaching the maximum stress. Compression in fiber and transverse direction was approximated by linear elastic-ideal plastic stress versus strain curves and no stress degradation. Overall, the material input was defined in a very similar way as shown before for the ballistic impact simulations with a different unidirectional composite. For the crush simulations, the equivalent erosion strain in the General Tabulated Failure Criterion was set to 0.6.

The tested component was a C-channel with a laminate layup of $[45, -45, 0, 90]_S$ that was crushed with an angle of the loading plate of 0°.

The total thickness of the 8 ply layup was 1.889mm. Figure 12 shows the simulation setup with the composite plate in red, the fixture plate on the bottom in yellow, and the transparent loading plate that was modeled using a rigid body. The plate was displaced in z-direction, as shown by the blue arrows, to crush the composite C-channel.

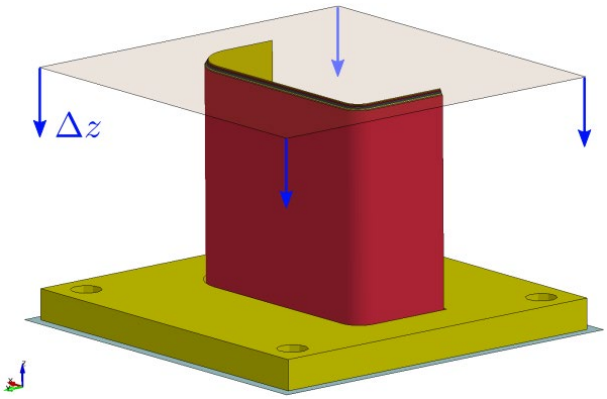

Figure 12: Crush simulation setup

When modeling composites with shell elements, there are two approaches that are commonly used. First, the different plies with their material orientation can be accounted for by defining a single element through the thickness and having different properties on an integration point level. Figure 13a shows the edge of the composite C-channel modeled with a single element through the thickness.

For a better distribution of the initial load, the plate was tapered at the top edge. This was modeled in the single element approach by defining a single ply for the top row of elements and two plies for the second row of elements until the full thickness of the plate was reached at the 8th element where all 8 plies were modeled with 8 integration points. With this modeling approach, delamination cannot be accounted for.

The second approach is to model the plies individually with one element per ply. Figure 13b shows the edge of the composite C-channel modeled following this approach. The first yellow layer of elements on the left represents the first 45° ply with the following other plies being slightly shorter to account for the tapering of the physical part. Delamination is accounted for by using a tiebreak contact between the individual plies.

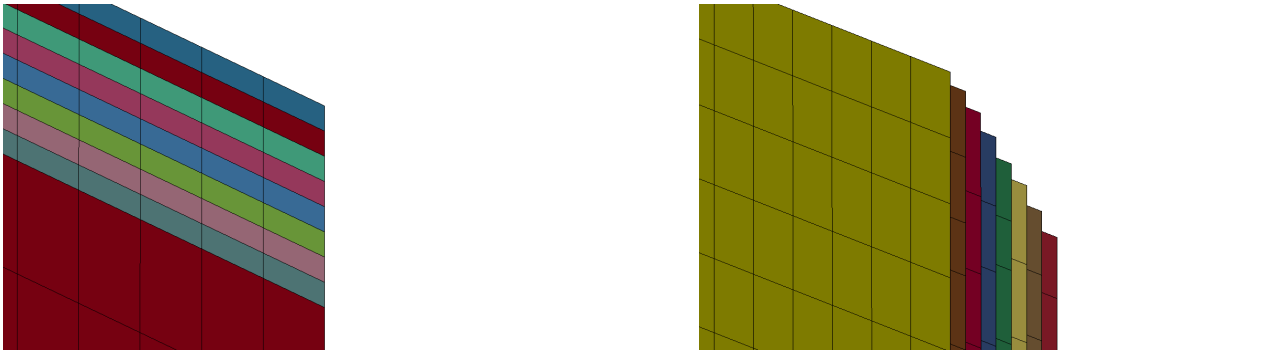

a) 1 element through the thickness, 8 integration points *b) 8 elements through the thickness, 2 integration points each*

Figure 13: C-Channel modeling techniques, edge view

Figure 14 shows the deformed geometries at the end of the crush simulations. Unfortunately, no images of the deformed geometry after the physical tests were available. On the left, in Figures 14a, 14c and 14e, the deformed geometry of the part simulated with MAT58 is shown.

The fringe colors represent the average amount of damage that has accumulated in the fiber direction in all through-thickness integration points on a scale from zero (blue) to one (red). The C-channel was highly damaged with significant stiffness degradation that extended far beyond the buckled areas. This highlights a potential shortcoming of the continuum damage model utilized in MAT58. Damage in MAT58 is fully coupled, meaning that loading in any material direction will influence the load bearing capabilities in all other directions.

When observing a physical composite material, however, it is highly unlikely that this is the case. Consider, for example, loading in tension 2-direction. This type of loading will likely not affect tension in the fiber direction, as the fibers would stay intact even at fracture. Using the same material input, the crush was also simulated using the modeling approach shown in Figure 13b.

As the MAT58 material card was optimized for the modeling technique with only one element through the thickness, the material parameters represented an average of the material behavior including delamination and averaging the effects of damage throughout the material. This led to forces that were significantly lower to what was measured in the test and, therefore, this modeling approach was abandoned for MAT58.

In the images on the right, Figures 14b, 14d and 14f, the deformed geometry obtained using the new material model (MAT213) is shown. The overall buckling modes in the simulations using the validated material model MAT58 and the new material model MAT213 are fairly similar. The maximum damage parameter (tension and shear) is fringe plotted on a scale from zero (blue) to 0.9 (red). Even though only the top and bottom plies are visible in this plot, damage obtained with the new material model is much more localized throughout all plies in the material. This seems to be a better representation of the physical composite material. Some localized delamination at the top of the C-channel can be seen and the part buckles in a more brittle manner when compared to MAT58, where the component folded more smoothly.

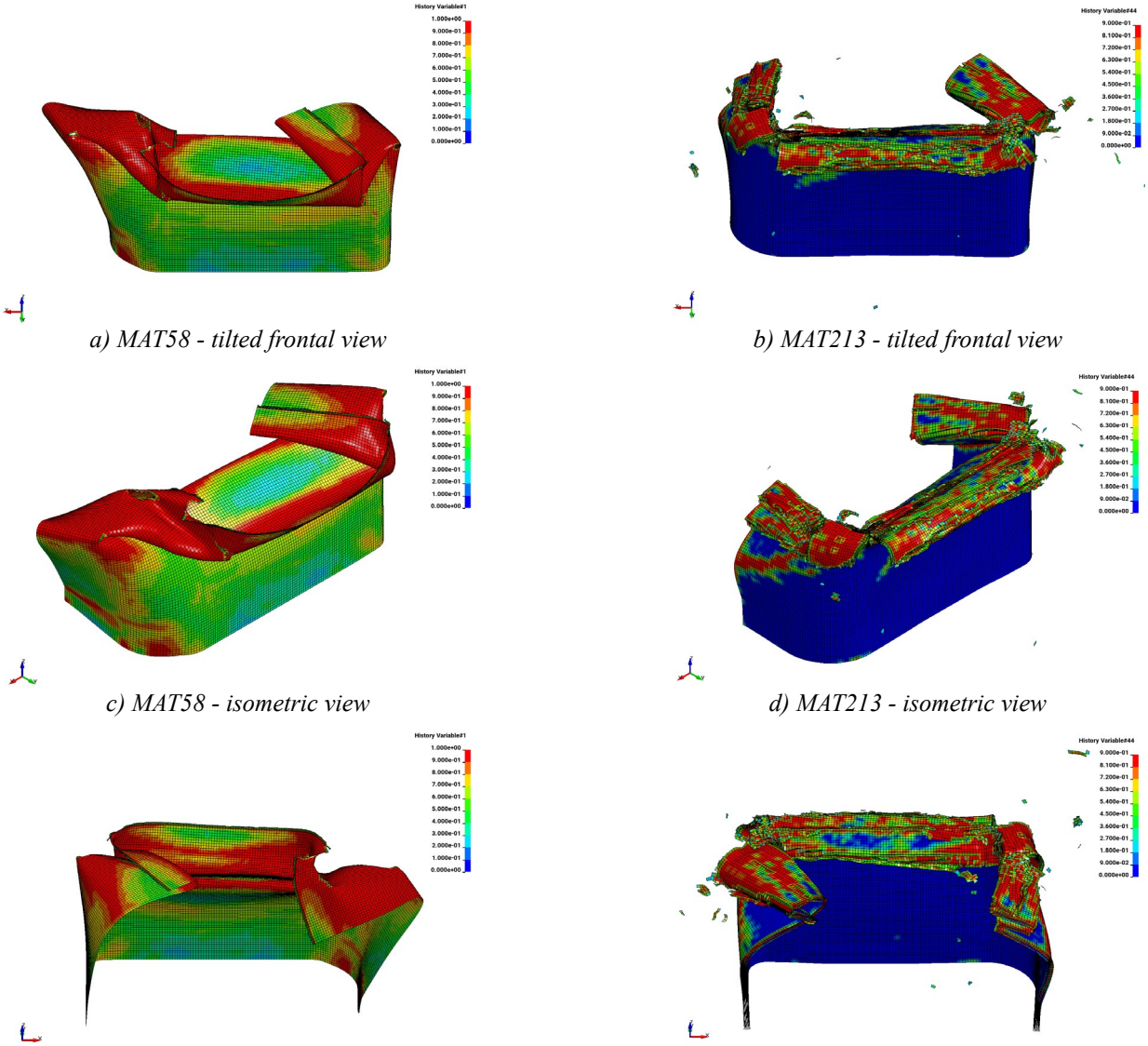

a) MAT58 - tilted frontal view

b) MAT213 - tilted frontal view

c) MAT58 - isometric view

d) MAT213 - isometric view

e) MAT58 - tilted rear view

f) MAT213 - tilted rear view

Figure 14: Comparison of C-channel crush simulations using MAT58 and MAT213

In Figure 15a the force versus displacement of the physical test specimen are shown as dotted black lines, while the baseline simulation using MAT58 is shown in green. The sudden increase of the force level in the MAT58 simulation can be attributed to the modeling technique with only one element through the thickness. The results using the new material model are shown in red with the maximum force matching the test results very well. Similar to the test, the force increased more slowly as the tapered top of the C-channel was loaded. The force in the tests then dropped to a level below what MAT213 predicted.

This part of the force versus displacement curve MAT58 matches fairly well, however, the later increase of force in the region between a displacement of 20mm and 45mm is not represented by the baseline simulation with MAT58. In the available physical test results, in this region of the curve, a large variation between test one and the tests two and three is apparent. This deviation between the different tests can most likely be attributed to different buckling modes and highlights the need for stochastic modeling capabilities in composites. With the new material model, a second peak of the force is visible between a displacement of 30 and 40mm.

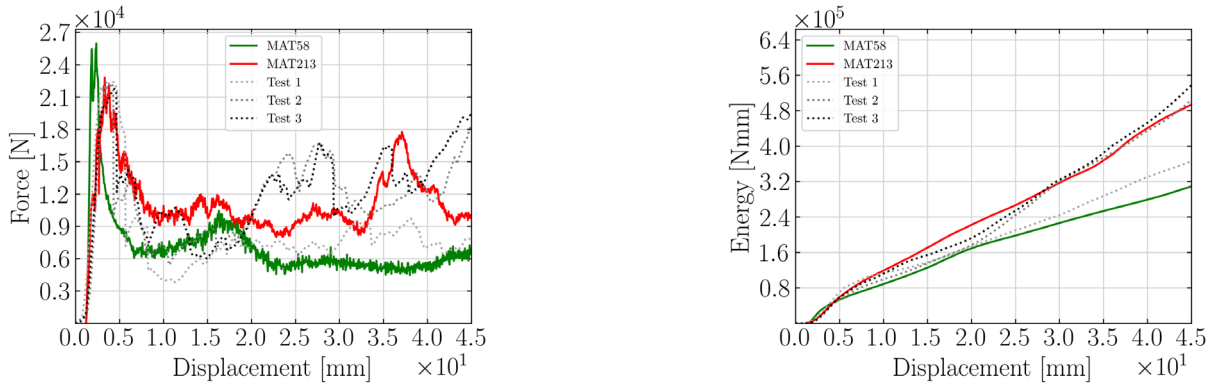

a) Force versus displacement *b) Absorbed energy versus displacement*

Figure 15: Comparison of crush simulations and test results

In automotive crush load cases, the energy absorbed by the component is of great importance. As much impact energy as possible should be absorbed by the crumple zone of the car. Figure 15b shows how much energy was absorbed by the composite C-Channel at any given displacement throughout the compressive loading. In tests two and three the absorbed energy was very similar, while the total absorbed energy in the first test was significantly lower. The difference in the test results can most likely be attributed to a different buckling mode that was excited in this test. This highlights the difficulty when dealing with composite materials, which often show a high variability in their material parameters and, consequently, in buckling and failure modes. The new material model matches the total absorbed energy in tests two and three quite accurately, while MAT58 under-predicts the total energy when compared to all three tests.

Even with the limited material test data available, a correlation was achieved between the test results and the simulation using the new material model. The overall buckling modes of the simulation with the new material model resembled the deformed geometry of the fully validated material (MAT58). With more available material test data available, the full potential of the newly developed material model can be utilized, and more predictive simulations will be possible.

References

[1] M. Melis, M. Pereira, R. K. Goldberg, and M. Rassaian, "Dynamic Impact Testing and Model Development in Support of NASA's Advanced Composites Program," in *2018 AIAA/ASCE/AHS/ASC Structures, Structural Dynamics, and Materials Conference*, Kissimmee, Florida, 2018, doi: 10.2514/6.2018-1699.

[2] B. Khaled *et al.*, "Experimental characterization of composites to support an orthotropic plasticity material model," *J. Compos. Mater.*, vol. 52, no. 14, pp. 1847–1872, Jun. 2018, doi: 10.1177/0021998317733319.

[3] S. Dong, A. Sheldon, and K. Carney, "Modeling of Carbon-Fiber-Reinforced Polymer (CFRP) Composites in LS-DYNA with Optimization of Material and Failure Parameters in LS-OPT®," p. 11, 2018.